Theoretical Chemistry Accounts (2023) 142:68
https://doi.org/10.1007/s00214-023-03007-7

RESEARCH

Generalization of the local diabatization approach for propagating electronic degrees of freedom in nonadiabatic dynamics

Mohammad Shakiba[1] · **Alexey V. Akimov**[1]

Received: 21 February 2023 / Accepted: 13 July 2023 / Published online: 30 July 2023

Abstract
In this Festschrift contribution in honor of Prof. Maurizio Persico, we present a systematic derivation and comprehensive assessment of several integrators for quantum–classical time-dependent Schrodinger (TD-SE) and Liouville (QCLE) equations. Our formalism is rooted in the basis set reprojection approach, but it naturally leads to a family of local diabatization (LD) integrators, including the one pioneered by Prof. Persico and co-workers. The formalism naturally accounts for trivial state crossing effects and helps solve related phenomena that often pose significant numerical problems in nonadiabatic molecular dynamics simulations. We adapt the LD-based methods for the QCLE integration. We generalize the symmetric splitting integrator proposed by one of us earlier and demonstrate how it can be applied to integrate both TD-SE and QCLE. Our analysis and computations suggest that the reprojection approach is critical for capturing correct qualitative dynamics in trivial crossing regimes, but the proper integration approach is still needed for high accuracy of calculations in general case. Our computations also reveal an interesting coherence discontinuity effect introduced by the LD approximation. We provide a detailed discussion of the algorithms and their implementation in the open-source Libra software and present their comprehensive assessment using several well-designed model problems.

Keywords Nonadiabatic dynamics · Quantum dynamics · Trajectory surface hopping · Electronic integrators · Trivial crossing · Local diabatization

1 Introduction

Nonadiabatic molecular dynamics (NA-MD) is a powerful tool to study the evolution of excited states, as relevant to photovoltaic [1–7], photocatalytic applications [8–11], and in biological systems [12–14]. While exact quantum dynamics is possible in certain low-dimensional systems [15–18], modeling it in extended systems requires approximate methods [19, 20]. The quantum–classical trajectory surface hopping (TSH) methods have been the most widely used and well-developed techniques [21–25]. Because of the complexity of the "zoo" of such approximate methods, the comprehensive and systematic assessment of various available options has been a long-standing and actively explored topic. In our efforts to this methodology assessment, we have developed an open-source code, called Libra [26, 27], that implements a large number of known schemes. Although such an assessment has been planned as one of our goals for this contribution, we found ourselves addressing another seemingly straightforward, but quite confusing topic—the proper integration of the time-dependent Schrodinger equation (TD-SE) underlying almost every NA-MD simulation technique. We further realized that this topic is an ideal fit as a contribution to the Festschrift in honor of Prof. Persico, hence we narrowed our initial scope to discussing integrators for TD-SE, as well as for quantum–classical Liouville's equation (QCLE).

Although the TD-SE or QCLE integration can be seen as a rather straightforward topic and has been described in various accounts [28], the formalism is somewhat more complicated in the presence of the so-called trivial crossings [29]. The latter occurs when two diabatic states cross but are not coupled or are weakly coupled (Fig. 1a). In this model problem, the adiabatic states coincide with the diabatic ones in the asymptotic regions. Since the adiabatic states are conventionally indexed according to their energies, one may encounter a situation when the

✉ Alexey V. Akimov
alexeyak@buffalo.edu

[1] Department of Chemistry, University at Buffalo, State University of New York, Buffalo, NY 14260, USA

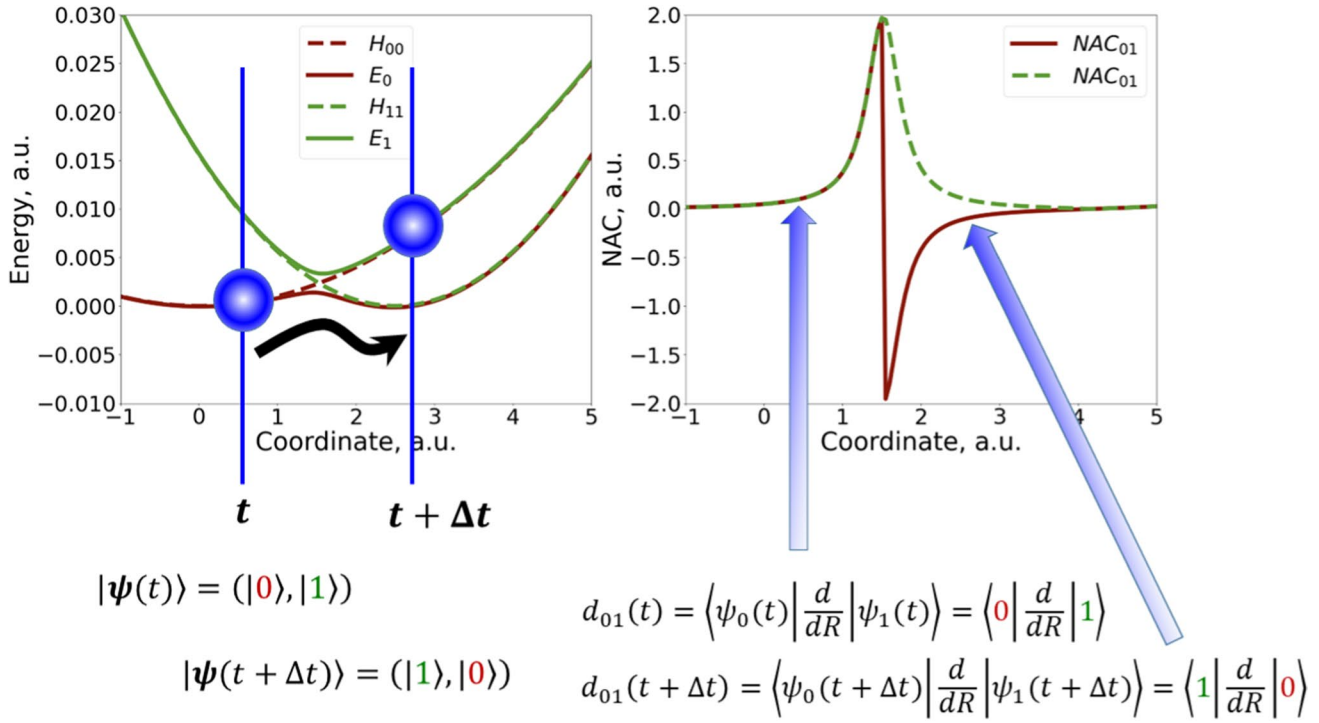

Fig. 1 The state identity change along a reaction coordinate. The elements in the vectors of state vectors $|\psi\rangle$ are ordered according to their adiabatic energies (as obtained from the adiabatic state calculations), but their diabatic character (as indicated by the color and the index of the most close diabatic state) may change. For instance, at time t, the lowest-energy adiabatic state $\psi_0(t)$ corresponds the "red" diabatic state $|0\rangle$. Past the intersection point, at time $t + \Delta t$, the same lowest-energy adiabatic basis state $\psi_0(t + \Delta t)$ is most close to the green diabatic state $|1\rangle$. As a result, $\langle\psi_0|\frac{d}{dR}|\psi_1\rangle$ corresponds to the couplings between differently ordered (permuted) adiabatic states at times t and $t + \Delta t$, leading to an unphysical abrupt change of NAC sign (the red curve in panel b). The NAC computed with the identity-ordered basis states should follow the dashed green curve

energy-ordered adiabatic states switch their identities (the mapping to the diabatic states). This state reordering occurs when the nuclear reaction coordinate passes the crossing point of the diabatic energy surfaces. For instance, consider the blue point in Fig. 1a. At the initial time t, it starts in the adiabatic state 0 (solid red line), which also coincides with the diabatic state 0 (the dashed red line). If the coupling of the diabatic surfaces is zero, the system should evolve on the diabatic surface 0 all the time, without switching to the diabatic state 1 (the dashed green line). However, during this motion, at time $t + \Delta t$, the diabatic state 0 corresponds to a higher-energy adiabatic state 1 (the solid green line). Thus, the evolution should lead to the oscillation of the population between the two adiabatic states, since the unchanged diabatic state maps onto different adiabatic states on the left and on the right sides of the crossing point. Vice versa, the same adiabatic state maps onto different diabatic states on the two sides of the crossing point. Hence, the adiabatic state changes its identity (the projection onto diabatic states). Hence, conducting even regular adiabatic dynamics would require accounting for the state identity change. In other words, there should be a mechanism for active state change even in case of "adiabatic" dynamics that is the one where only one adiabatic state (although of different identity and energy ordering) is used. Simply forcing the dynamics to stay on the same-energy ordering state (e.g., the lowest-energy state) would lead to qualitatively incorrect results, as apparent from analyzing the schematic in Fig. 1.

To date, several algorithms have been designed for state tracking and handling the trivial crossing situation. These developments include the min-cost algorithm of Fernandez-Alberti and Tretiak [29] as well as a similar approach of Ryabinkin and Izmaylov [30], the internal-consistency check by Wang and Prezhdo [31], our stochastic state tracking algorithm [32], and the local diabatization (LD) approach of Granucci, Persico, and co-workers [33, 34]. Alternatively, Meek and Levine proposed the norm-conserving interpolation (NPI) procedure to correctly integrate TD-SE in the conical intersection regions [35]. The complexity of the TD-SE integration problem is further hardened by the phase inconsistency problem in adiabatic representation that arises due to the fact that at every time step, the adiabatic basis functions are defined up to an arbitrary complex phase, which can randomly vary from geometry to geometry. The phase correction problem has been addressed in the works of

Subotnik [36], Gonzalez [37], as well as in an earlier work by one of us [38].

In previous accounts, we have detailed the phase consistency and state tracking corrections [39]. However, the resulting scheme is still rather cumbersome and requires a lot of bookkeeping, which results in a less readable and less transferable code. In the present work, we approach the problem of the phase consistency correction and state identity tracking from the conceptually satisfying viewpoint of a basis re-expansion. This re-expansion approach is also motivated by the recently presented integrator for the quantum trajectory with adaptive Gaussians (QTAG) methodology [40] as well as by the TD-SE integration in a quasi-diabatic basis [41]. Although we rely on the well-known ideas, we use them to develop a unified and self-consistent formalism for state tracking and phase correction. As an application of our formalisms, we demonstrate how one can derive a series of new integrators for the TD-SE, one of which turns out to be the LD approach of Granucci, Persico and co-workers [33, 34]. We further extend our formalism to the integration of the QCLE. We present integrators for TD-SE and QCLE that are based on either matrix exponents or on geometric Trotter-splitting-based approach, reported earlier by one of us [42]. In this account, we generalize the latter approach to the case of Hamiltonian/Liouvillian operators with nonzero real components of the off-diagonal elements. We demonstrate the applicability of such generalization to integrating both the TD-SE and QCLE. Finally, we conduct a comprehensive comparison of all the integration schemes with several model Hamiltonians designed to induce several dynamical regimes in electron-nuclear dynamics.

2 Theory and methods

2.1 Brief overview of NA-MD theory

The main goal of many quantum dynamics methods is to solve the time-dependent Schrodinger equation (TD-SE):

$$i\hbar\frac{\partial|\Psi\rangle}{\partial t}=\widehat{H}|\Psi\rangle, \tag{1}$$

where $\widehat{H}$ is the system's Hamiltonian, $\hbar$ is the reduced Planck's constant ($\hbar=1$, in atomic units), and $|\Psi\rangle$ the wavefunction of the system. One can further specify a representation of the wavefunction, to include electronic or nuclear degrees of freedom, to use the position or momentum representation, or to represent it in the basis of adiabatic or diabatic states [43]. In this account, we focus on quantum–classical approaches, such as TSH or Ehrenfest methods, so the dependence of wavefunctions on nuclear degrees of freedom is given via swarms of such trajectories, and the wavefunction $|\Psi\rangle$ is the electronic wavefunction in the position representation. Furthermore, we consider that this wavefunction can be represented in the basis of adiabatic ("adi", $|\boldsymbol{\psi}_{\text{adi}}\rangle$) or diabatic ("dia", $|\boldsymbol{\psi}_{\text{dia}}\rangle$) states:

$$|\Psi\rangle=|\boldsymbol{\psi}_{\text{adi}}\rangle C_{\text{adi}}=|\boldsymbol{\psi}_{\text{dia}}\rangle C_{\text{dia}}. \tag{2}$$

Here, we adopt the vector or state vectors notation, discussed in more detail in Ref. 43. Within this notation, the bolded fonts represent vectors, including the vectors of state vectors, that is: $|\boldsymbol{\psi}\rangle=\left(|\psi_0\rangle,|\psi_1\rangle,\ldots,|\psi_{N-1}\rangle\right)$. The capital Latin letters denote matrices, that is: $C=\left(c_0,c_1,\ldots,c_{N-1}\right)^T$ is a column-vector of the basis state amplitudes, C_{adi} or C_{dia}. The matrix representation of operators can be conveniently written as:

$$A_{\text{rep}}=\langle\boldsymbol{\psi}_{\text{rep}}|\widehat{A}|\boldsymbol{\psi}_{\text{rep}}\rangle, rep=adi,dia,\ldots. \tag{3}$$

The basis states of the two representations are related by the basis transformation matrix, U:

$$|\boldsymbol{\psi}_{\text{adi}}\rangle=|\boldsymbol{\psi}_{\text{dia}}\rangle U. \tag{4}$$

We also introduce the following objects: the overlap in the diabatic basis, $S=\langle\boldsymbol{\psi}_{\text{dia}}|\boldsymbol{\psi}_{\text{dia}}\rangle$, the time-overlap matrix, $P(t,t+\Delta t)=\langle\boldsymbol{\psi}_{\text{adi}}(t)|\boldsymbol{\psi}_{\text{adi}}(t+\Delta t)\rangle$, the time-derivative coupling, $D_{\text{rep}}=\langle\boldsymbol{\psi}_{\text{rep}}|\frac{\partial}{\partial t}\boldsymbol{\psi}_{\text{rep}}\rangle$, electronic Hamiltonian matrices, $H_{\text{rep}}=\langle\boldsymbol{\psi}_{\text{rep}}|\widehat{H}|\boldsymbol{\psi}_{\text{rep}}\rangle$ and the vibronic Hamiltonian matrices, $H_{\text{vib}}^{\text{rep}}=H_{\text{rep}}-i\hbar D_{\text{rep}}$. Finally, it is worth noting that by virtue of orthonormality of the adiabatic basis, $\langle\boldsymbol{\psi}_{\text{adi}}|\boldsymbol{\psi}_{\text{adi}}\rangle=I$, one gets, $U^{+}SU=I$, from which $U^{-1}=U^{+}S$.

Alternative to the TD-SE, one can solve the quantum Liouville equation (QLE):

$$i\hbar\frac{\partial\widehat{\rho}}{\partial t}=\left[\widehat{H},\widehat{\rho}\right]. \tag{5}$$

for the density matrix operator, $\widehat{\rho}$. For closed systems, the density matrix operator can be represented as:

$$\widehat{\rho}=|\Psi\rangle\langle\Psi|. \tag{6}$$

We focus on quantum–classical methods, in which the wavefunction or the density matrix elements depend functionally on the electronic degrees of freedom (DOF), $\boldsymbol{r}$, but parametrically on the nuclear DOFs, $\boldsymbol{R}$, that is: $|\Psi\rangle=|\Psi(\mathbf{r},\mathrm{t};\mathbf{R}(\mathrm{t}))\rangle$, or $\widehat{\rho}=\widehat{\rho}(t,\boldsymbol{r};\boldsymbol{R}(t))$. The evolution of the nuclear DOFs is done classically or semi-classically, as will be discussed below.

2.2 General considerations for electronic DOFs integration

Projecting the TD-SE, Eq. (1), onto the basis of diabatic or adiabatic states, one can obtain equations for evolving amplitudes:

$$i\hbar\frac{\partial C_{\mathrm{adi}}}{\partial t} = E_{\mathrm{adi}}C_{\mathrm{adi}} - i\hbar D_{\mathrm{adi}}C_{\mathrm{adi}} = \left[E_{\mathrm{adi}} - i\hbar D_{\mathrm{adi}}\right]C_{\mathrm{adi}} = H^{\mathrm{adi}}_{\mathrm{vib}}C_{\mathrm{adi}}, \tag{7a}$$

$$i\hbar S\frac{\partial C_{\mathrm{dia}}}{\partial t} = H_{\mathrm{dia}}C_{\mathrm{dia}} - i\hbar D_{\mathrm{dia}}C_{\mathrm{dia}} = \left[H_{\mathrm{dia}} - i\hbar D_{\mathrm{dia}}\right]C_{\mathrm{dia}} = H^{\mathrm{dia}}_{\mathrm{vib}}C_{\mathrm{dia}}, \tag{7b}$$

where

$$E_{\mathrm{adi}} = \langle\boldsymbol{\psi}_{\mathrm{adi}}\left|\widehat{H}\right|\boldsymbol{\psi}_{\mathrm{adi}}\rangle = U^{+}\langle\boldsymbol{\psi}_{\mathrm{dia}}\left|\widehat{H}\right|\boldsymbol{\psi}_{\mathrm{dia}}\rangle U = U^{+}H_{\mathrm{dia}}U. \tag{8}$$

As is discussed in Section S1 of the Supporting Information, Eqs. (7a) and (7b) are equivalent to each other. That is in the absence of any other differences (e.g., in handling nuclear dynamics or any stochastic events), the electronic evolution computed in any of the two representations should be identical. However, although the equations are identical, their solutions (once converted back to one of the two representations) are not, due to numerical approximations as well as due to potential state reordering/phase inconsistency of the basis states computed in different representations (section S2 of the Supporting Information). Indeed, the integration of Eq. (7) can be conducted in a formal way:

$$\begin{aligned} C_{\mathrm{adi}}(t+\Delta t) &\approx \exp\left(-\frac{i}{\hbar}\Delta t H^{\mathrm{adi}}_{\mathrm{vib}}\left(t+\frac{\Delta t}{2}\right)\right) \\ C_{\mathrm{adi}}(t) &\approx \exp\left(-\frac{i}{2\hbar}\Delta t\left[H^{\mathrm{adi}}_{\mathrm{vib}}(t) + H^{\mathrm{adi}}_{\mathrm{vib}}(t+\Delta t)\right]\right)C_{\mathrm{adi}}(t), \end{aligned} \tag{9a}$$

$$\begin{aligned} C_{\mathrm{dia}}(t+\Delta t) &\approx \exp\left(-\tfrac{i}{\hbar}\Delta t\left[S^{-1}\left(t+\tfrac{\Delta t}{2}\right)H^{\mathrm{dia}}_{\mathrm{vib}}\left(t+\tfrac{\Delta t}{2}\right)\right]\right)C_{\mathrm{dia}}(t) \\ &\approx \exp\left(-\tfrac{i}{2\hbar}\Delta t\left[S^{-1}(t)H^{\mathrm{dia}}_{\mathrm{vib}}(t) + S^{-1}(t+\Delta t)H^{\mathrm{dia}}_{\mathrm{vib}}(t+\Delta t)\right]\right)C_{\mathrm{dia}}(t). \end{aligned} \tag{9b}$$

Note that the first approximation in each equation corresponds to a mid-point rule and would require additional evaluation of the Hamiltonian and diabatic overlap matrix elements at the mid-point, which adds the computational expenses. The last approximation in each of Eq. (9) is derived assuming a linear interpolation of the integrand in the exponential operator (Sect. 3 of the Supporting Information). Note that such an assumption is not valid in regions of strong nonadiabatic coupling (NAC), where the coupling elements exhibit a Lorentzian dependence. Analyzing Eq. (9), one can see that Eq. (9b) is not sensitive to state reordering/phase changes problem since it involves only diabatic properties, which as always well-behaved by the definition. On the contrary, Eq. (9a) utilizes the adiabatic vibronic Hamiltonians, which may be affected by the above problems as demonstrated in Fig. 1, and hence corrections of the wavefunctions and derived properties are needed. Indeed, the character of adiabatic basis states may change past the point of diabatic surfaces intersection such that effective order of the basis function is changed (Fig. 1a), as elaborated in the Introduction. As a consequence, the derivative couplings may exhibit an abrupt change of sign, which corresponds to an effective permutation of the adiabatic states (Fig. 1b).

2.3 Integrators for the TD-SE

We are primarily interested in integrating the TD-SE, Eq. (1), in the adiabatic representation since it is in this case when pathological situations of state identity switch (trivial crossings) and state phase inconsistencies may reveal themselves. Formally integrating Eq. (1), yields:

$$\begin{aligned} |\Psi(\mathrm{t}+\Delta\mathrm{t})\rangle &= |\boldsymbol{\psi}_{\mathrm{adi}}(\mathrm{t}+\Delta\mathrm{t})\rangle C_{\mathrm{adi}}(t+\Delta\mathrm{t}) \\ &= \left[\int_0^{\Delta t} \mathrm{d}\tau \exp\left(-\frac{i\tau}{\hbar}\widehat{H}(t+\tau)\right)\right]|\Psi(\mathrm{t})\rangle, \end{aligned} \tag{10a}$$

or

$$\begin{aligned} C_{\mathrm{adi}}(t+\Delta t) = \langle\boldsymbol{\psi}_{\mathrm{adi}}(t+\Delta t)| \\ \left[\int_0^{\Delta t} \mathrm{d}\tau \exp\left(-\frac{i\tau}{\hbar}\widehat{H}(t+\tau)\right)\right]|\boldsymbol{\psi}_{\mathrm{adi}}(\mathrm{t})\rangle C_{\mathrm{adi}}(t). \end{aligned} \tag{10b}$$

Computing the integral in Eq. (10b) requires preserving the order and phases of the basis functions at every instant of the $[t, t+\Delta t]$ integral. However, the basis functions $|\boldsymbol{\psi}_{\mathrm{adi}}(t)\rangle$ and $|\boldsymbol{\psi}_{\mathrm{adi}}(t+\Delta t)\rangle$ may change their relative order (e.g., in trivial crossing situations) or acquire a spurious phase difference. To conduct a correct integration, we switch to the dynamically consistent basis, $|\widetilde{\boldsymbol{\psi}}_{\mathrm{adi}}(t)\rangle$, constructed to have no such problems, that is:

$$\langle\widetilde{\boldsymbol{\psi}}_{\mathrm{adi}}(t)|\widetilde{\boldsymbol{\psi}}_{\mathrm{adi}}(t+\Delta t)\rangle \approx I. \tag{11}$$

Note that although the integration is conducted in the $|\widetilde{\boldsymbol{\psi}}_{\mathrm{adi}}\rangle$ basis, the observables of interest (e.g., density matrix and state populations or energies, etc.) are computed in the original "globally adiabatic" basis, $|\boldsymbol{\psi}_{\mathrm{adi}}\rangle$.

Apparently, the wavefunction should be invariant with respect to the choice of the basis, so Eq. (2) can be extended to:

$$|\Psi\rangle = |\widetilde{\boldsymbol{\psi}}_{\mathrm{adi}}(t)\rangle\widetilde{C}_{\mathrm{adi}}(t) = |\boldsymbol{\psi}_{\mathrm{adi}}(t)\rangle C_{\mathrm{adi}}(t). \tag{12}$$

Let's assume the cumulative (encumbered for the whole duration, t, since the very beginning of simulation) transformation between ordered and "raw" bases is given by a projector matrix $T(t)$:

$$|\widetilde{\boldsymbol{\psi}}_{\text{adi}}(t)\rangle = |\boldsymbol{\psi}_{\text{adi}}(t)\rangle T(t), \tag{13a}$$

$$|\boldsymbol{\psi}_{\text{adi}}(t)\rangle = |\widetilde{\boldsymbol{\psi}}_{\text{adi}}(t)\rangle T^{-1}(t). \tag{13b}$$

Hence,

$$C_{\text{adi}}(t) = T(t)\widetilde{C}_{\text{adi}}(t), \tag{14a}$$

$$\widetilde{C}_{\text{adi}}(t) = T^{-1}(t)C_{\text{adi}}(t). \tag{14b}$$

Note that the definition of the projector matrix T in Eq. (13) is inverse of the one used in the definition of the local diabatic matrix in the works of Persico, $T = T^{-1}_{\text{Persico}}$. [33]

As demonstrated in section S4 of the Supporting Information, the best choice of the matrices $T(t)$ and $T(t+\Delta t)$ at the ends of each integration intervals $[t, t+\Delta t]$ is:

$$T(t) = I, \tag{15a}$$

$$T(t+\Delta t) = P^{-1}(t, t+\Delta t)\Big(\big[P^{-1}(t, t+\Delta t)\big]^{+} P^{-1}(t, t+\Delta t)\Big)^{-1/2}. \tag{15b}$$

With the help of the projector matrix T defined in Eq. (15), one can formulate various approximations to evaluate Eq. (10b) and hence construct various integrators. For instance, using the result Eq. (S10), one obtains $\left[\int_0^{\Delta t} \mathrm{d}\tau \exp\left(-\frac{i\tau}{\hbar}\widehat{H}(\tau)\right)\right] \approx \left[\exp\left(-\frac{i\Delta t}{2\hbar}\left[\widehat{H}(t) + \widehat{H}(t+\Delta t)\right]\right)\right]$. The latter operator can be approximated using either a crude splitting, Eq. (16a) or a symmetric Trotter splitting, Eq. (16b):

$$\left[\exp\left(-\frac{i\Delta t}{2\hbar}\left[\widehat{H}(t) + \widehat{H}(t+\Delta t)\right]\right)\right] \approx \left[\exp\left(-\frac{i\Delta t}{2\hbar}\widehat{H}(t+\Delta t)\right)\right]\left[\exp\left(-\frac{i\Delta t}{2\hbar}\widehat{H}(t)\right)\right]. \tag{16a}$$

$$\left[\exp\left(-\frac{i\Delta t}{2\hbar}\left[\widehat{H}(t) + \widehat{H}(t+\Delta t)\right]\right)\right] \approx \left[\exp\left(-\frac{i\Delta t}{4\hbar}\widehat{H}(t)\right)\right] \left[\exp\left(-\frac{i\Delta t}{2\hbar}\widehat{H}(t+\Delta t)\right)\right]\left[\exp\left(-\frac{i\Delta t}{4\hbar}\widehat{H}(t)\right)\right]. \tag{16b}$$

Equation (16a) can be interpreted as: the evolution of the amplitudes is guided by the $\widehat{H}(t)$ on the interval $\left[t, t+\frac{\Delta t}{2}\right]$ and by the $\widehat{H}(t+\Delta t)$ on the interval $\left[t+\frac{\Delta t}{2}, t+\Delta t\right]$ as illustrated in Fig. 2a. With these approximations, Eq. (16), the amplitudes are propagated according to Eq. (17), respectively (see Sect. 5 of the Supporting Information for the detailed derivation):

$$C_{\text{adi}}(t+\Delta t) = A(t+\Delta t)T(t+\Delta t)A(t)C_{\text{adi}}(t), \tag{17a}$$

$$C_{\text{adi}}(t+\Delta t) = T(t+\Delta t)B(t)T^{+}(t+\Delta t)A(t+\Delta t)T(t+\Delta t)B(t)C_{\text{adi}}(t), \tag{17b}$$

with

$$A(t) = \langle \boldsymbol{\psi}_{\text{adi}}(t)|\left[\exp\left(-\frac{i\Delta t}{2\hbar}\widehat{H}(t)\right)\right]|\boldsymbol{\psi}_{\text{adi}}(\text{t})\rangle = \exp\left(-\frac{i\Delta t}{2\hbar}H(t)\right), \tag{18a}$$

$$B(t) = \langle \boldsymbol{\psi}_{\text{adi}}(t)|\left[\exp\left(-\frac{i\Delta t}{4\hbar}\widehat{H}(t)\right)\right]| \boldsymbol{\psi}_{\text{adi}}(t)\rangle = \exp\left(-\frac{i\Delta t}{4\hbar}H(t)\right) = A^{1/2}. \tag{18b}$$

The graphical representation of the constructed propagators is shown in Fig. 2 with a trivial crossing model. In this model, the diabatic coupling is zero, so the system that is initialized

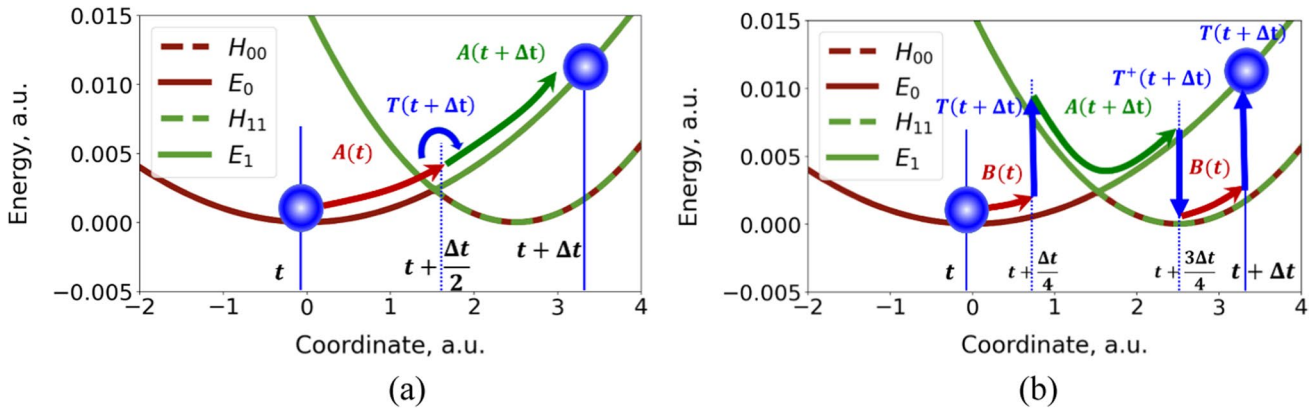

Fig. 2 Graphical representation of the integrators in Eq. (17): (**a**) the integrator Eq. (17a); (**b**) the integrator Eq. (17b). Arrows represent the exponential operators acting on the corresponding adiabatic surfaces: red—the adiabatic surface 0, green—the adiabatic surface 1; the time in parenthesis indicates at which time steps the surfaces 0 or 1 are considered. The operator A propagates for $\Delta t/2$ time duration, while the operator B propagates only for $\Delta t/4$ time duration

on the left parabola should stay evolving on that parabola. In this example, one starts on the lower adiabatic state at $q \approx 0$, which also corresponds to the initialization on the diabatic surface 0 (left parabola, dashed red curve, which is hidden behind the solid lines). The integrator Eq. (17a) evolves the quantum amplitudes on the lower adiabatic state on the time-interval of $\left[t, t+\frac{\Delta t}{2}\right]$, following the operator $A(t)$ (the red arrow). This evolution coincides with the evolution on the lower diabatic surface. The trivial crossing is identified according to Eq. (15b), leading to $T(t+\Delta t) \approx \begin{pmatrix} 0 & 1 \\ 1 & 0 \end{pmatrix}$, which switches the populations of the ground and excited adiabatic states. In other words, the amplitude of the adiabatic state 0 will be placed to the position of the state 1 by the operator $T(t+\Delta t)$ (the blue arrow), and vice versa for the amplitude of the adiabatic state 1. Finally, the new amplitude of state 1 will be propagated using properties of the adiabatic surface 1, which corresponds to operator $A(t+\Delta t)$ (the green arrow). This motion is also consistent with the expected motion on the left parabola (diabatic surface 0). Thus, the algorithm shall correctly describe the populations switching in the adiabatic representation, while keeping the diabatic populations unchanged. The graphical illustration of the integrator in Eq. (17b) is shown in Fig. 2b and can be interpreted in similar terms.

2.4 Derivations of the Trotter-splitting-based rotations propagator for solving the TD-SE and alike equations

The operators A and B in Eq. (18) are defined as the matrix exponentials and can be computed using eigenvalues and eigenvectors of the corresponding Hamiltonian matrices (the approach used in the present work) or direct summation of the Taylor series with matrix operands. However, the action of such exponential matrices is to essentially solve a first-order ordinary differential equations of the TD-SE type. As was demonstrated earlier, such an integration can be done without resorting to the matrix eigenvalue problem, by using the Trotter-like splitting of the corresponding evolution operator [28]. The resulting propagator can be represented in terms of complex phase accumulation (due to diagonal elements of Hamiltonian matrix) and rotations in complex 2D planes (due to imaginary off-diagonal terms proportional to nonadiabatic couplings). In certain situations, the off-diagonal elements of the effective Hamiltonian matrices can also contain real components, e.g., diabatic couplings or when representing Liouvillian operator in tetradic notation (see below). Here we extend the previous algorithm [28] to such situation.

We aim to integrate the TD-SE-like equation:

$$i\hbar\frac{\partial C}{\partial t} = XC. \tag{19}$$

Here, X is an effective Hamiltonian, which could be the vibronic Hamiltonian that includes nonadiabatic couplings. We also assume that this effective Hamiltonian is Hermitian, $X = X^{+}$. The amplitudes C are understood more generally than wavefunction amplitudes. With the matrix elements written as:

$$X_{ij} = \mathrm{Re}\left[X_{ij}\right] + i\mathrm{Im}\left[X_{ij}\right], \tag{20}$$

The Hermiticity condition is equivalent to: $\mathrm{Re}\left[X_{ij}\right] = \mathrm{Re}\left[X_{ji}\right]$ and $\mathrm{Im}\left[X_{ij}\right] = -\mathrm{Im}\left[X_{ji}\right]$, the properties to be used below. The formal solution of Eq. (19) on the interval $[t, t+\Delta t]$ is:

$$C(t+\Delta t) = \exp(iL\Delta t)C(t). \tag{21}$$

Here, iL is the effective Liouville's operator given by:

$$iL \equiv \dot{C}\frac{\partial}{\partial C} = \sum_i \dot{C}_i \frac{\partial}{\partial C_i}. \tag{22}$$

Keeping in mind Eq. (20) and the Hermiticity conditions above, iL can be written as:

$$\begin{aligned} iL &= -\frac{i}{\hbar}\sum_i\sum_j X_{ij}C_j\frac{\partial}{\partial C_i} = -\frac{i}{\hbar}\sum_{i,j} X_{ij}C_j\frac{\partial}{\partial C_i} \\ &= -\frac{i}{\hbar}\sum_i X_{ii}C_i\frac{\partial}{\partial C_i} - \frac{i}{\hbar}\sum_{i,j:i>j}\left[X_{ij}C_j\frac{\partial}{\partial C_i}\right] - \frac{i}{\hbar}\sum_{i,j:i<j}\left[X_{ij}C_j\frac{\partial}{\partial C_i}\right] \\ &= -\frac{i}{\hbar}\sum_i X_{ii}C_i\frac{\partial}{\partial C_i} - \frac{i}{\hbar}\sum_{i,j:i>j}\left[X_{ij}C_j\frac{\partial}{\partial C_i}\right] - \frac{i}{\hbar}\sum_{i,j:i>j}\left[X_{ji}C_i\frac{\partial}{\partial C_j}\right] \\ &= -\frac{i}{\hbar}\sum_i X_{ii}C_i\frac{\partial}{\partial C_i} - \frac{i}{\hbar}\sum_{i,j:i>j}\left[X_{ij}C_j\frac{\partial}{\partial C_i} + X_{ji}C_i\frac{\partial}{\partial C_j}\right]. \end{aligned} \tag{23}$$

The terms in the last sum can be simplified as:

$$\begin{aligned} X_{ij}C_j\frac{\partial}{\partial C_i} - X_{ji}C_i\frac{\partial}{\partial C_j} &= \left[\mathrm{Re}\left(X_{ij}\right) + i\mathrm{Im}\left(X_{ij}\right)\right]C_j\frac{\partial}{\partial C_i} \\ &\quad - \left[\mathrm{Re}\left(X_{ji}\right) + i\mathrm{Im}\left(X_{ji}\right)\right]C_i\frac{\partial}{\partial C_j} \\ &= \mathrm{Re}\left(X_{ij}\right)\left[C_j\frac{\partial}{\partial C_i} + C_i\frac{\partial}{\partial C_j}\right] \\ &\quad + i\mathrm{Im}\left(X_{ij}\right)\left[C_j\frac{\partial}{\partial C_i} - C_i\frac{\partial}{\partial C_j}\right]. \end{aligned} \tag{24}$$

So, the overall operator can be written as:

$$
\begin{aligned}
iL &= -\frac{i}{\hbar}\sum_i X_{ii}C_i\frac{\partial}{\partial C_i} - \frac{i}{\hbar}\sum_{i,j:i>j}\left[\mathrm{Re}\left(X_{ij}\right)\left[C_j\frac{\partial}{\partial C_i} + C_i\frac{\partial}{\partial C_j}\right]\right.\\
&\quad \left. + i\mathrm{Im}\left(X_{ij}\right)\left[C_j\frac{\partial}{\partial C_i} - C_i\frac{\partial}{\partial C_j}\right]\right]\\
&= \sum_i iL_i^{(1)} + \sum_{i,j:i>j} iL_{ij}^{(2)} + \sum_{i,j:i>j} iL_{ij}^{(3)}.
\end{aligned}
\tag{25}
$$

$$
iL_i^{(1)} = -\frac{i}{\hbar}X_{ii}C_i\frac{\partial}{\partial C_i}, \tag{26a}
$$

$$
iL_{ij}^{(2)} = \frac{\mathrm{Im}\left(X_{ij}\right)}{\hbar}\left[C_j\frac{\partial}{\partial C_i} - C_i\frac{\partial}{\partial C_j}\right], \tag{26b}
$$

$$
iL_{ij}^{(3)} = -\frac{i\mathrm{Re}\left(X_{ij}\right)}{\hbar}\left[C_j\frac{\partial}{\partial C_i} + C_i\frac{\partial}{\partial C_j}\right]. \tag{26c}
$$

The action of the first operator, $iL^{(1)}$, is trivial:

$$
\exp\left(iL_i^{(1)}\Delta t\right)C_i = \exp\left(-\frac{i\Delta t}{\hbar}X_{ii}\right)C_i. \tag{27a}
$$

The action of the other two operators can be derived as:

$$
\begin{aligned}
&\exp\left(iL_{ij}^{(2)}\Delta t\right)\begin{pmatrix}C_i\\C_j\end{pmatrix}\\
&= \begin{pmatrix}C_i\\C_j\end{pmatrix} + A\begin{pmatrix}C_j\\-C_i\end{pmatrix} + \frac{A^2}{2!}\begin{pmatrix}-C_i\\-C_j\end{pmatrix}\\
&\quad + \frac{A^3}{3!}\begin{pmatrix}-C_j\\C_i\end{pmatrix} + \frac{A^4}{4!}\begin{pmatrix}C_i\\C_j\end{pmatrix}\cdots\\
&= \begin{pmatrix}1-\frac{A^2}{2!}+\frac{A^4}{4!}\cdots & A-\frac{A^3}{3!}+\cdots\\ -A+\frac{A^3}{3!}+\cdots & 1-\frac{A^2}{2!}+\frac{A^4}{4!}\cdots\end{pmatrix}\begin{pmatrix}C_i\\C_j\end{pmatrix}\\
&= \begin{pmatrix}\cos(A) & \sin(A)\\ -\sin(A) & \cos(A)\end{pmatrix}\begin{pmatrix}C_i\\C_j\end{pmatrix},
\end{aligned}
\tag{27b}
$$

and

$$
\begin{aligned}
\exp\left(iL_{ij}^{(3)}\Delta t\right)\begin{pmatrix}C_i\\C_j\end{pmatrix} &= \begin{pmatrix}C_i\\C_j\end{pmatrix} - iB\begin{pmatrix}C_j\\C_i\end{pmatrix} + \frac{(-iB)^2}{2!}\begin{pmatrix}C_i\\C_j\end{pmatrix} + \frac{(-iB)^3}{3!}\begin{pmatrix}C_j\\C_i\end{pmatrix} + \frac{(-iB)^4}{4!}\begin{pmatrix}C_i\\C_j\end{pmatrix} + \cdots\\
&= \begin{pmatrix}1-\frac{B^2}{2!}+\frac{B^4}{4!}+\cdots & -iB+\frac{(-iB)^3}{3!}+\cdots\\ -iB+\frac{(-iB)^3}{3!}+\cdots & 1-\frac{B^2}{2!}+\frac{B^4}{4!}+\cdots\end{pmatrix}\begin{pmatrix}C_i\\C_j\end{pmatrix}\\
&= \begin{pmatrix}\cos(B) & -i\sin(B)\\ -i\sin(B) & \cos(B)\end{pmatrix}\begin{pmatrix}C_i\\C_j\end{pmatrix}.
\end{aligned}
\tag{27c}
$$

Here,

$$
A = \frac{Im\left(X_{ij}\right)\Delta t}{\hbar}, \tag{28a}
$$

$$
B = \frac{Re\left(X_{ij}\right)\Delta t}{\hbar}. \tag{28b}
$$

All the operators are unitary and norm-conserving, so the resulting integration schemes shall be stable and robust, even with large integration time steps.

Finally, we can write down the final factorization:

$$
\begin{aligned}
\exp(iL\Delta t) &= \exp\left(\left\{\sum_i iL_i^{(1)} + \sum_{i,j:i>j} iL_{ij}^{(2)} + \sum_{i,j:i>j} iL_{ij}^{(3)}\right\}\Delta t\right)\\
&\approx \left\{\prod_i \exp\left(iL_i^{(1)}\frac{\Delta t}{2}\right)\right\}\left\{\prod_{i,j:i>j}\exp\left(iL_{ij}^{(3)}\frac{\Delta t}{2}\right)\right\}\\
&\quad \left\{\prod_{i,j:i>j}\exp\left(iL_{ij}^{(2)}\frac{\Delta t}{2}\right)\right\}\\
&\quad \left\{\prod_{O\{i,j:i>j\}}\exp\left(iL_{ij}^{(2)}\frac{\Delta t}{2}\right)\right\}\left\{\prod_{O\{i,j:i>j\}}\exp\left(iL_{ij}^{(3)}\frac{\Delta t}{2}\right)\right\}\\
&\quad \left\{\prod_{O\{i\}}\exp\left(iL_i^{(1)}\frac{\Delta t}{2}\right)\right\}
\end{aligned}
\tag{29}
$$

Here, the notation $O\{i,j:i>j\}$ indicates the ordering that is opposite to that taken in the previous double sums such that the overall splitting is symmetric. As an example, for a 3-state system, the factorization would be:

$$
\begin{aligned}
&\exp\left(iL_0^{(1)}\frac{\Delta t}{2}\right)\exp\left(iL_1^{(1)}\frac{\Delta t}{2}\right)\exp\left(iL_2^{(1)}\frac{\Delta t}{2}\right)\\
&\exp\left(iL_{01}^{(3)}\frac{\Delta t}{2}\right)\exp\left(iL_{02}^{(3)}\frac{\Delta t}{2}\right)\exp\left(iL_{12}^{(3)}\frac{\Delta t}{2}\right)\\
&\exp\left(iL_{01}^{(2)}\frac{\Delta t}{2}\right)\exp\left(iL_{02}^{(2)}\frac{\Delta t}{2}\right)\exp\left(iL_{12}^{(2)}\frac{\Delta t}{2}\right)\\
&\exp\left(iL_{12}^{(2)}\frac{\Delta t}{2}\right)\exp\left(iL_{02}^{(2)}\frac{\Delta t}{2}\right)\exp\left(iL_{01}^{(2)}\frac{\Delta t}{2}\right)\\
&\exp\left(iL_{12}^{(3)}\frac{\Delta t}{2}\right)\exp\left(iL_{02}^{(3)}\frac{\Delta t}{2}\right)\exp\left(iL_{01}^{(3)}\frac{\Delta t}{2}\right)\\
&\exp\left(iL_2^{(1)}\frac{\Delta t}{2}\right)\exp\left(iL_1^{(1)}\frac{\Delta t}{2}\right)\exp\left(iL_0^{(1)}\frac{\Delta t}{2}\right)
\end{aligned}
\tag{30}
$$

2.5 Integrators for the QCLE

Alternative to the TD-SE, electronic DOFs can be described in terms of the density matrix. In this case, we need integrators for the QCLE:

$$\frac{\partial\widehat{\rho}}{\partial t} = -\frac{i}{\hbar}\left[\widehat{H},\widehat{\rho}\right] = -\frac{i}{\hbar}\left[\widehat{H}\widehat{\rho} - \widehat{\rho}\widehat{H}\right] = -\frac{i}{\hbar}\widehat{L}\widehat{\rho}. \tag{31}$$

Here, we consider closed quantum systems, for which the density matrix operator, $\widehat{\rho} = |\Psi\rangle\langle\Psi|$ can be represented in the basis of adiabatic or diabatic states $\widehat{\rho} = |\boldsymbol{\psi}_{\text{rep}}\rangle C_{\text{rep}} C^{+}_{\text{rep}}\langle\boldsymbol{\psi}_{\text{rep}}|$.

In the dynamically consistent basis, the QCLE can be written explicitly in a tetradic notation [44] as:

$$\frac{\partial\widetilde{\rho}_{ij}}{\partial t} = -\frac{i}{\hbar}\sum_{a,b}\widetilde{L}_{ij,ab}\widetilde{\rho}_{ab}, \tag{32}$$

where

$$\widetilde{L}_{ij,ab} = \widetilde{H}_{ia}\delta_{bj} - \widetilde{H}_{bj}\delta_{ai}. \tag{33}$$

Here,

$$\widetilde{H} = \langle\widetilde{\boldsymbol{\psi}}|\widehat{H}|\widetilde{\boldsymbol{\psi}}\rangle = T^{+}\langle\boldsymbol{\psi}|\widehat{H}|\boldsymbol{\psi}\rangle T, \tag{34}$$

is the Hamiltonian in the dynamically consistent basis. Equations similar to Eqs. (32) and (33) are derived in Sect. 6 of the Supporting Information. Initially, the Liouvillian operator is constructed using the vibronic Hamiltonian, H_{vib}. However, since the integration is done in the locally diabatic (aka dynamically consistent) basis, the NACs can be neglected, so the $\widetilde{H}_{\text{vib}} \to \widetilde{H}$.

To integrate Eq. (32), we recast it in a matrix form:

$$\frac{\partial vec(\widetilde{\rho})}{\partial t} = -i\widetilde{L}vec(\widetilde{\rho}), \tag{35a}$$

Here, $\widetilde{L}$ is $N^2 \times N^2$ Liovillian super-matrix, and $vec()$ is a vectorization operation of the matrix, converting a $N \times N$ matrix into a $N^2 \times 1$ vector. So:

$$vec\left(\widetilde{\rho}(t+\Delta t)\right) = \left[\int_0^{\Delta t} d\tau \exp\left(-\frac{i\tau}{\hbar}\widetilde{L}(t+\tau)\right)\right] vec(\widetilde{\rho}(t)). \tag{35b}$$

Since the QCLE and the TD-SE are equivalent for closed systems, the following transformations hold:

$$\rho_{\text{adi}} = C_{\text{adi}}C^{+}_{\text{adi}} = T\widetilde{C}_{\text{adi}}\widetilde{C}^{+}_{\text{adi}}T^{+} = T\widetilde{\rho}_{\text{adi}}T^{+}, \tag{36a}$$

$$\widetilde{\rho}_{\text{adi}} = T^{-1}\rho_{\text{adi}}\left(T^{+}\right)^{-1} = T^{+}\rho_{\text{adi}}T. \tag{36b}$$

The basis transformation matrices T can be computed analogously to the above prescriptions for the TD-SE formalism. In this case, we still need the time-overlap matrices, which are the wavefunction-derived properties. Considering that $T(t) = I$ for each integration time-interval, $[t, t+\Delta t]$, Eq. (35b) can be rewritten in terms of the original density matrix:

$$\rho(t+\Delta t) = T(t+\Delta t)vec^{-1} \left\{\left[\int_0^{\Delta t} d\tau \exp\left(-\frac{i\tau}{\hbar}\widetilde{L}(t+\tau)\right)\right] vec(\rho(t))T\right\} T^{+}(t+\Delta t). \tag{37}$$

The action of the operator $\left[\int_0^{\Delta t} d\tau \exp\left(-\frac{i\tau}{\hbar}\widetilde{L}(t+\tau)\right)\right]$ can be computed following any recipes already discussed in Sect. 2.3 with the exponential operators computed either directly or via rotation-based algorithms discussed in Sect. 2.4. Specifically, we consider:

$$\left[\int_0^{\Delta t} d\tau \exp\left(-\frac{i\tau}{\hbar}\widetilde{L}(\tau)\right)\right] \approx \left[\exp\left(-\frac{i\Delta t}{\hbar}\widetilde{L}\left(t+\frac{\Delta t}{2}\right)\right)\right], \tag{38}$$

with $\widetilde{L}\left(t+\frac{\Delta t}{2}\right)$ derived according to Eq. (33) from the $\widetilde{H}\left(t+\frac{\Delta t}{2}\right) \approx \frac{\widetilde{H}(t)+\widetilde{H}(t+\Delta t)}{2} = \frac{H(t)+T^{+}(t+\Delta t)H(t+\Delta t)T(t+\Delta t)}{2}$.

2.6 Summary of electronic DOF integration algorithms

The above formal approaches can be summarized in several explicit computational schemes that we assess in this work (Table 1). All the integrators are implemented in the open-source Libra package, starting from version v5.4.0. [45]

The integrators 1 and 2 are already defined by Eqs. (17a) and (17b), respectively. We also consider the original LD approach, scheme 3, given by Eq. (39):

$$C_{\text{adi}}(t+\Delta t) = T(t+\Delta t)\exp\left(-\frac{i\Delta t}{2\hbar}\left[H(t) + T^{+}(t+\Delta t)H(t+\Delta t)T(t+\Delta t)\right]\right) C_{\text{adi}}(t). \tag{39}$$

In it, apart from the final basis reprojection operation given by the matrix $T(t+\Delta t)$, the exponential operator is evaluated using the mid-point average of the Hamiltonians at the limiting points of the integration interval, that is using $H(t)$ and $H(t+\Delta t)$. However, the Hamiltonian at the end-point $t+\Delta t$ is similarity-transformed by the matrix $T(t+\Delta t)$ to account for possible basis states reordering and any spurious phase inconsistencies. For all integrators 1–3, the electronic Hamiltonian rather than vibronic Hamiltonian are used in the exponential operators to reflect the vanishing nature of the nonadiabatic terms as introduced by the LD approximation.

We also consider several heuristic, potentially naïve schemes, although corrected to account for the basis re-expansion. These integrators, 4–6, are given by Eqs. (40)–(42), respectively. In these methods, we opt to use vibronic Hamiltonians instead of the electronic ones even though the LD is assumed to be in effect. This is a scheme

Table 1 Integration schemes for electronic DOF

Integrator #	Integrator description
1	LD with crude splitting using matrix exponential, Eq. (17a)
2	LD with symmetric splitting using matrix exponential, Eq. (17b)
3	LD of Granucci and Persico using matrix exponential, Eq. (39)
4	1-point integration with H_{vib} and matrix exponential, Eq. (40)
5	Naïve mid-point integration with H_{vib} and matrix exponential, Eq. (41)
6	Mid-point integration with H_{vib} and similarity transformation of the second point and matrix exponential, Eq. (42)
7	Same as 1, but with rotation-based decomposition of propagator
8	Same as 2, but with rotation-based decomposition of propagator
9	Same as 3, but with rotation-based decomposition of propagator
10	Same as 4, but with rotation-based decomposition of propagator
11	Same as 5, but with rotation-based decomposition of propagator
12	Same as 6, but with rotation-based decomposition of propagator
13	Adiabatic Liouville integrator using matrix exponential, Eqs. (37), (38)
14	Same as 14, but with rotation-based decomposition of propagator

that one could potentially think of if not paying attention to the neglect of the NAC terms by the LD approximation. On the other hand, this approximation neglects NACs only approximately, so including them may be not as naïve as we state. The scheme 4, Eq. (40), evaluates the propagator using the vibronic Hamiltonian at the beginning point, that's where it needs no corrections since, by definition, we start with the correctly ordered states:

$$C_{\text{adi}}(t+\Delta t) = T(t+\Delta t)\exp\left(-\frac{i\Delta t}{\hbar}H_{\text{vib}}(t)\right)C_{\text{adi}}(t). \tag{40}$$

The scheme 5, Eq. (41) utilizes that mid-point rule to approximate $H_{\text{vib}}(t+\frac{\Delta t}{2})$ in a somewhat naïve way: $H_{\text{vib}}\left(t+\frac{\Delta t}{2}\right) \approx \frac{1}{2}\left[H_{\text{vib}}(t)+H_{\text{vib}}(t+\Delta t)\right]$. This mid-point approximation should be valid most of the time, except for the points where state reordering occurs, near avoided or trivial crossing points. At the same time, the NACs are likely to be small in the points where the mid-point approximation is valid and large at the points of avoided or trivial crossing. Thus, we anticipate that this scheme 5 may be less accurate than even the 1-point scheme 4.

$$C_{\text{adi}}(t+\Delta t) = T(t+\Delta t)\exp\left(-\frac{i\Delta t}{2\hbar}\left[H_{\text{vib}}(t)+H_{\text{vib}}(t+\Delta t)\right]\right)C_{\text{adi}}(t). \tag{41}$$

Further, we consider scheme 6, Eq. (42), which is identical to scheme 5 with the only exception that the H_{vib} is corrected for potential state crossings/phase effects at the end of the integration interval by the corresponding similarity transformation: $H_{\text{vib}}(t+\Delta t) \to T^{+}(t+\Delta t)H_{\text{vib}}(t+\Delta t)T(t+\Delta t)$. This scheme is similar to the original LD approach of Granucci, Persico, and Toniolo, Eq. (39), with the only exception that the vibronic Hamiltonian is used instead of the electronic one:

$$C_{\text{adi}}(t+\Delta t) = T(t+\Delta t)\exp\left(-\frac{i\Delta t}{2\hbar}\left[H_{\text{vib}}(t)+T^{+}(t+\Delta t)H_{\text{vib}}(t+\Delta t)T(t+\Delta t)\right]\right)C_{\text{adi}}(t). \tag{42}$$

2.7 Integrating nuclear DOF; overall integration schemes

All electronic integration algorithms are combined with the nuclear DOF integrator based on the Trotter symmetric splitting, yielding essentially the velocity form of the Verlet algorithm [46], Eqs. (43a), (43b), (43e). The integration of electronic variables is done directly after the call of the "update_Hamiltonian_variables" function, Eq. (43c), that recomputes wavefunctions, diabatic/adiabatic Hamiltonians and other derived properties such as forces in response to the update of nuclear coordinates, Eq. (43b). At this point, all the properties at time steps t and $t+\Delta t$ are known and can be used in the electronic DOF integration by the "propagate_electronic" function, Eq. (43d). This function computes the re-projection matrices, $P(t, t+\Delta t)$ and uses them in the electronic DOF integration algorithms discussed in Sects. 2.3–2.6.

$$p\left(t+\frac{\Delta t}{2}\right) = p(t)+F(t)\frac{\Delta t}{2}, \tag{43a}$$

$$q(t+\Delta t) = q(t)+M^{-1}p(t)\Delta t, \tag{43b}$$

Table 2 Parameters of the model Hamiltonians used in this work

Model	E_0, a.u	E_1, a.u	q_0, a.u	q_1, a.u	k_0, a.u	k_1, a.u	V_{01}, a.u
1	0.0	0.0	0.0	2.5	0.002	0.005	0.000
2	0.0	0.0	0.0	2.5	0.002	0.005	0.001
3	0.0	0.0	0.0	2.5	0.002	0.005	0.01
4	0.0	− 0.01	0.0	0.5	0.002	0.008	0.001

$$F(t+\Delta t), H(t+\Delta t), \boldsymbol{\psi}(t+\Delta t) = \text{call "}update\_Hamiltonian\_variables(q(t+\Delta t))\text{"}, \tag{43c}$$

$$call\text{ "}propagate\_electronic\text{"}, \tag{43d}$$

$$p(t+\Delta t) = p\left(t+\frac{\Delta t}{2}\right) + F(t+\Delta t)\frac{\Delta t}{2}, \tag{43e}$$

3 Computational details

The developed integrators are assessed using model Hamiltonians of the Holstein type. In diabatic representation, the Hamiltonian matrix elements are given by:

$$H_{\text{dia}} = \begin{pmatrix} E_0 + \frac{1}{2}k_0(q-q_0)^2 & V_{01} \\ V_{01} & E_1 + \frac{1}{2}k_1(q-q_1)^2 \end{pmatrix}. \tag{44}$$

We consider four models with the parameters (Table 2) chosen to mimic certain dynamical situation (Fig. 3). Specifically, Model 1 features a pure case of trivial crossing, zero diabatic coupling. Model 2 corresponds to an intermediate value of the diabatic coupling, leading to a strongly nonadiabatic model. Model 3 has a large value of diabatic coupling and hence corresponds to a mainly adiabatic case. Lastly, Model 4 parameters are chosen similar to those of Model 2, but such that two regions of nonadiabatic coupling are accessible to the dynamics yielded by the initial conditions we select. This model introduces stronger possibility of quantum wavepacket interferences and enhances any complications of the dynamics due to decoherence effects. Both Models 2 and 4 would be the great testbeds for benchmarking decoherence correction algorithms for nonadiabatic dynamics. The numerical values of the parameters in all four models are chosen to be on the order of magnitude of typical molecular potentials so that the dynamics would occur on typical molecular time scales of femto- to picoseconds.

In all calculations, we use only one electron-nuclear trajectory since we aim to assess the deterministic integration algorithms, so no averaging over stochastic parameters or processes is needed. In all simulations, the initial nuclear coordinate and momentum is chosen as $q(0) = -4.0$, $p(0) = 0.0$ so that the simulations starts far from the region of nonadiabatic coupling. In this region, the diabatic and adiabatic representation are nearly identical, which facilitates the comparison of the results of integration in different representations. Nuclear mass is chosen to be $m = 2000.0$ a.u. No randomization of the initial nuclear position or momentum is conducted as would be done in typical quantum–classical simulation (with multiple trajectories). This is done to ensure the possibility of the point-by-point comparison of the dynamics produced by different computational schemes. We note that our selection of $q(0)$ and $p(0)$ gives the system enough total energy to overcome the barriers and to visit regions of strong nonadiabatic coupling. Thus, our simulations are not biased to only show the regions of weak nonadiabatic coupling (where the dynamics would be largely adiabatic and the trivial crossing situation won't be realized). At the same time, we don't give the system too much total energy so that we aren't limited by the numerical limitations on the parameters Δt too early on.

We initialize the electronic coefficients on the lowest adiabatic state, such that $C_{\text{adi}}(0) = \begin{pmatrix} 1.0+0.0i \\ 0.0+0.0i \end{pmatrix}$. No random phase is given to the electronic amplitudes so that simulations with all methods and integration time steps could be compared to each other directly. The dynamics is evolved for 25,000.0 a.u. of time with the integration time steps, Δt, of 0.001, 0.005, 0.01, 0.05, 0.1, 0.5, 1.0, 2.0, 5.0, 10.0, 20.0, 40.0, 50.0, 100.0, and 200.0 a.u. We build different recipes based on the integration schemes introduced above (Table 1).

The error of each integration scheme (which includes both the methodology selection and the choice of Δt) is calculated as a time-integral of the absolute deviation of the density matrix elements, $\rho_{ij}(t)$, from the reference values at the same time-points, $\overline{\rho}_{ij}(t)$:

$$e = \frac{1}{T}\sum_{ij}\int_0^T dt\left|\rho_{ij}(t) - \overline{\rho}_{ij}(t)\right|^2 \approx \frac{1}{N+1}\sum_{n=0}^{N}\sum_{i,j}\left|\rho_{ij}(n\cdot\Delta t) - \overline{\rho}_{ij}(n.\Delta t)\right|^2. \tag{45}$$

Here, $\rho_{ij}(t) = \rho_{ij}(n\Delta t) = \rho_{ij}(n, \Delta t)$ indicates the elements of the density matrix computed using one of the integration schemes and $\overline{\rho}_{ij}(t)$ is the reference density matrix with $\Delta t = 0.001$ a.u. The reference calculations are based on integrating the TD-SE in diabatic representation (where

no approximations like LD are needed) and converting the corresponding density matrix to the adiabatic representation. Since the accuracy of the time-integral Eq. (45) itself may depend on Δt, we choose to use the right-hand side of Eq. (45) as the error measure, leaving the integral in that equation only as a physical motivation for defining such an error measure. As another way to remove the numerical dependence of the error measure, Eq. (45), on the time-discretization step, Δt, we evaluate Eq. (45) at the fixed set of time-points for all integration schemes. This is done to prevent a situation when ρ would be available at some time point if a smaller Δt is used, and not available when a larger Δt is used. Thus, the set of the points, at which the evaluation of the terms entering Eq. (45) is conducted, is determined by the largest Δt. Finally, since the error measure defined in Eq. (45) is based on density matrices, it equally suited for the TD-SE and the QCLE integration scheme. Defining an alternative error measure based solely on the wavefunction amplitudes won't work for our purposes of comprehensive assessment of distinct types of integration schemes.

4 Results and discussion

Our main results are summarized in Fig. 4. When comparing the integration errors as the function of the integration time step, Δt (Fig. 4), we observe that all methods fall into one of the two groups. The first one is the one where electronic Hamiltonian is used in either the TD-SE (cases 1–3, 7–9) or the QCLE (cases 13–14) integration. All such schemes show relatively small errors, nearly identical to each other, for all the used Δt values. This means that: (1) all the variants of the LD integration are accurate and comparable to each other in accuracy; (2) the rotation-based propagators are as good as those based on computing matrix exponentials; (3) all of these currently implemented TD-SE and QCLE integrators (Cases 1, 2, 3, 7, 8, 9, 13, and 14) yield comparable accuracy and can be used interchangeably. For integrators in this group, the error varies from 10^{-27} (trivial models and small Δt) to 10^{-3} (for any model and the largest values of Δt). Such errors can be considered acceptable, even for large values of Δt. From the practical standpoint, one is free to use any of them even though some appear to be more sophisticated.

The second group of integration schemes includes all variants using vibronic Hamiltonian (cases 4–6 and 10–12). In these schemes, the TD-SE or QCLE are integrated using the traditional vibronic Hamiltonian, H_{vib} (that explicitly depends on nonadiabatic coupling), instead of electronic Hamiltonians alone (as done in the LD-based methods). The error values start from 10^{-3} values, in the adiabatic dynamics (Model 3) and hold until reasonable integration time steps on the order of $\Delta t \approx 10$ a.u. Such accuracy is also achieved even when the smallest integration time step of $\Delta t = 0.001$ a.u. is used and is comparable to the worst errors of the LD-based integrators used even with the largest time steps of 100 a.u. The only reason why such heuristic integration schemes work reasonably in this case is because the NACs are small, so the difference between electronic and vibronic Hamiltonians is small. Another situation where the heuristic integrators work as good as the proper LD schemes, is the case of pure trivial crossing (Model 1). In this case, the NAC is zero everywhere except for the exact point of the diabatic surfaces crossing, which may be difficult to "hit" exactly in numerical calculations. Furthermore, in our implementation, the NAC for models like Model 1 (constant diabatic coupling) is set to zero when the energy gap is below 10^{-25} a.u., to avoid the division by zero. Thus, staying on the same-index adiabatic state is the expected outcome of the traditional NAC-based (or H_{vib}-based) integration of the TD-SE for such a model. However, the correct behavior for this model is to observe Rabi oscillations of the adiabatic populations, while having unchanged diabatic population on the starting diabatic state. This is where the basis set reprojection, Eqs. (13)–(14), plays a critical role. It is this reprojection that enables the correct "switch" of the active adiabatic state (and the corresponding TD-SE amplitudes' adjustment), leading to small errors for Model 1. In the strongly nonadiabatic Models 2 and 4, the error measure of the heuristic integrators starts at values as large as 1.0 even for the smallest Δt used. Thus, such integrators are not suitable for integrating the TD-SE and the QCLE. We should note that in our implementation the reprojection approach is used with the H_{vib}-based integrators as a way to track the evolution of the basis states. However, unlike the trivial crossing Model 1, even the basis reprojection is not sufficient to yield low errors in the dynamics. This is because the NAC terms of the H_{vib} matrices used in the integrators are inconsistent with the LD assumption.

We further comment on several interesting observations regarding the error measure vs. Δt. First, for all integrators we generally observe the expected increase of the error with the integration time step. For proper LD integrators, we observe two critical regions—first, at Δt around 0.01 a.u., where we observe a rather significant "jump" of the error from nearly numerically exact integration (errors on the order of $10^{-27} - 10^{-15}$) to an approximate solution (errors on the order 10^{-7}). Further increasing Δt up to about 10 a.u. leads to a steady increase of the error up to still-acceptable level of 10^{-3}. Although both nuclear and electronic DOF integration are affected by Δt, the nuclear integration is likely to be less sensitive to such small integration time steps. Thus, the error accumulation in this region can be attributed mostly to the electronic integration schemes. This is where we observe either a steady increase of the error (for the proper LD integration scheme) or a complete insensitivity of the error to Δt (for the heuristic schemes).

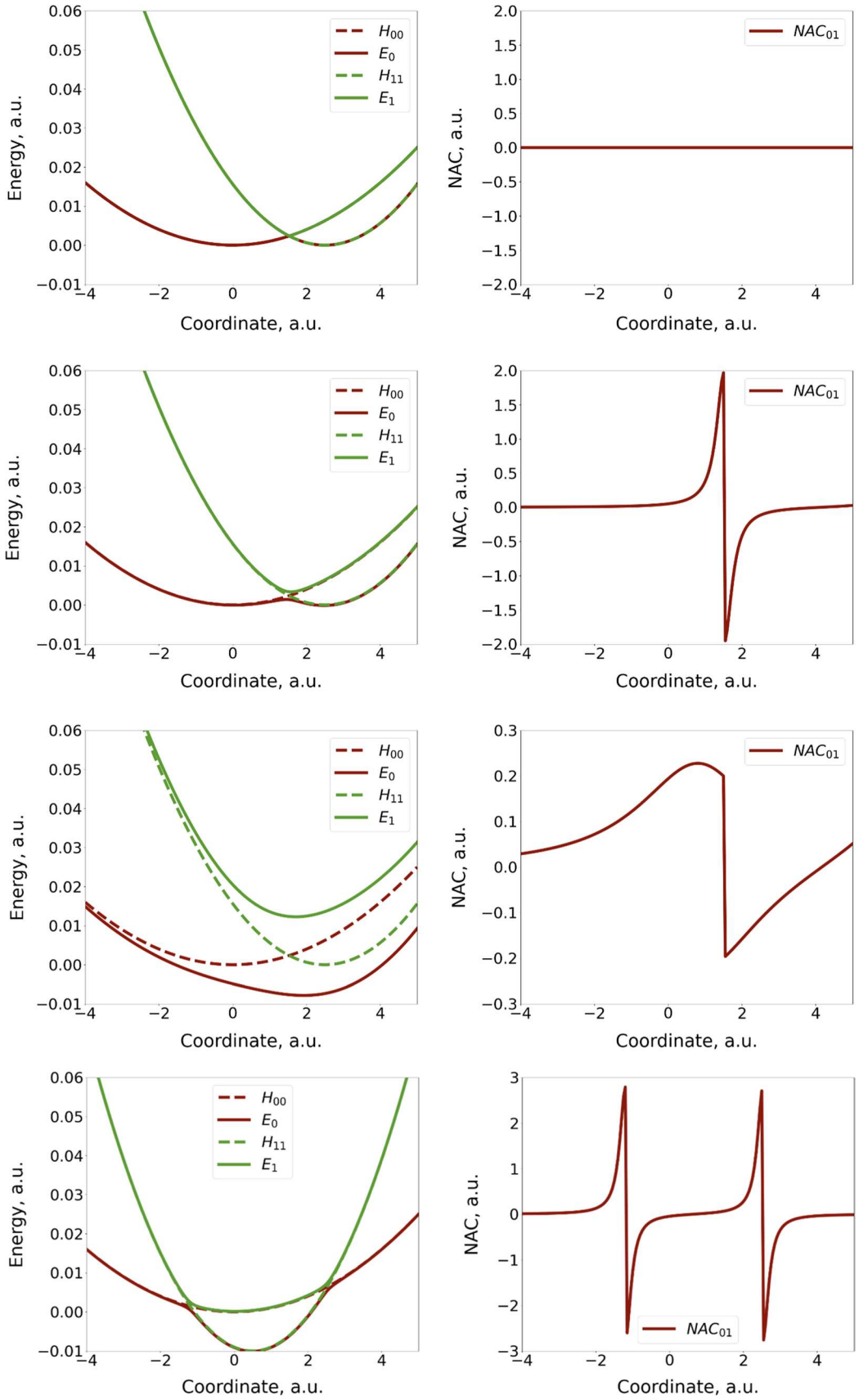

◂**Fig. 3** The four 2-level Holstein-type models used in this work. Each row represents a model, from 1 to 4. The first column shows diabatic (the dashed lines) and adiabatic (the solid lines) energy surfaces for the models. The second column shows the "raw" derivative couplings computed along the nuclear coordinate

The second critical region is met at Δt values around 10–100 a.u. This is where we observe a second "jump" in the error's order of magnitude. This jump is less pronounced for the proper LD algorithms and is very rapid for the heuristic schemes. We associate this effect with the errors due to nuclear DOF integration, which could strongly affect the NAC values and hence lead to faster accumulation of error in the heuristic methods that rely on the vibronic Hamiltonians. Interestingly, for the nonadiabatic Model 2 (and partially for Model 4), we observe a drop of error when Δt increases past this second critical point around 10 a.u. This effect may be attributed to the decreased changes for system to sample regions near the state crossing and increased changes of sampling regions with smaller NACs instead. As a result, the H_{vib} in such simulations is closer to H on average, so the heuristic integration scheme converges to the proper LD one.

As demonstrated above, the variety of the LD-based integrators are derived starting from the basis set reprojection approach described in the theory section. Although the new integrators derived do not yield significant practical advantage over the original LD approach of Granucci, Persico and Toniolo (which itself is one case of such a family of integrators), the fact that they all work well confirms that the introduced framework is correct and can be used to derive other schemes, if needed. Furthermore, we want to highlight the importance of the reprojection matrix resets to the identity matrix at every nuclear iteration. As discussed in section S4 of the Supporting Information, in our early formulations, we used the cumulative reprojection matrix which was propagated along the TD-SE amplitudes. However, such an approach led to a very fast accumulation of errors, due to neglect of the time-dependence of certain terms. As a result, the obtained dynamics was incorrect. For example, the Rabi

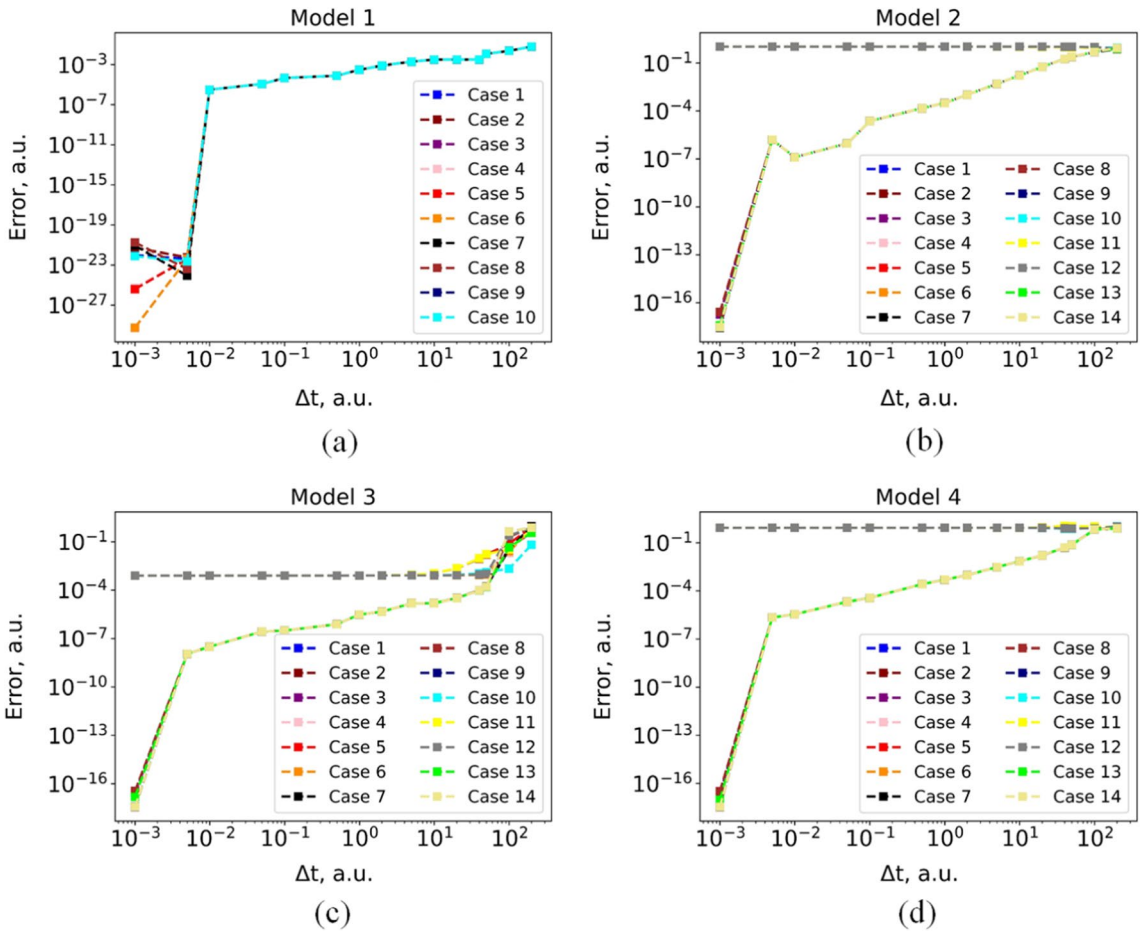

Fig. 4 Computed errors between the density matrix of each integrator and the reference density matrix for (**a**) Model 1, (**b**) Model 2, (**c**) Model 3, and (**d**) Model 4. For all models, but Model 1, the results fall into two groups leading to sets of nearly overlapping lines. The first set (accurate ones) includes cases 1, 2, 3, 7, 8, 9, 13 and 14. The second set (inaccurate) includes cases 4, 5, 6, 10, 11, and 12

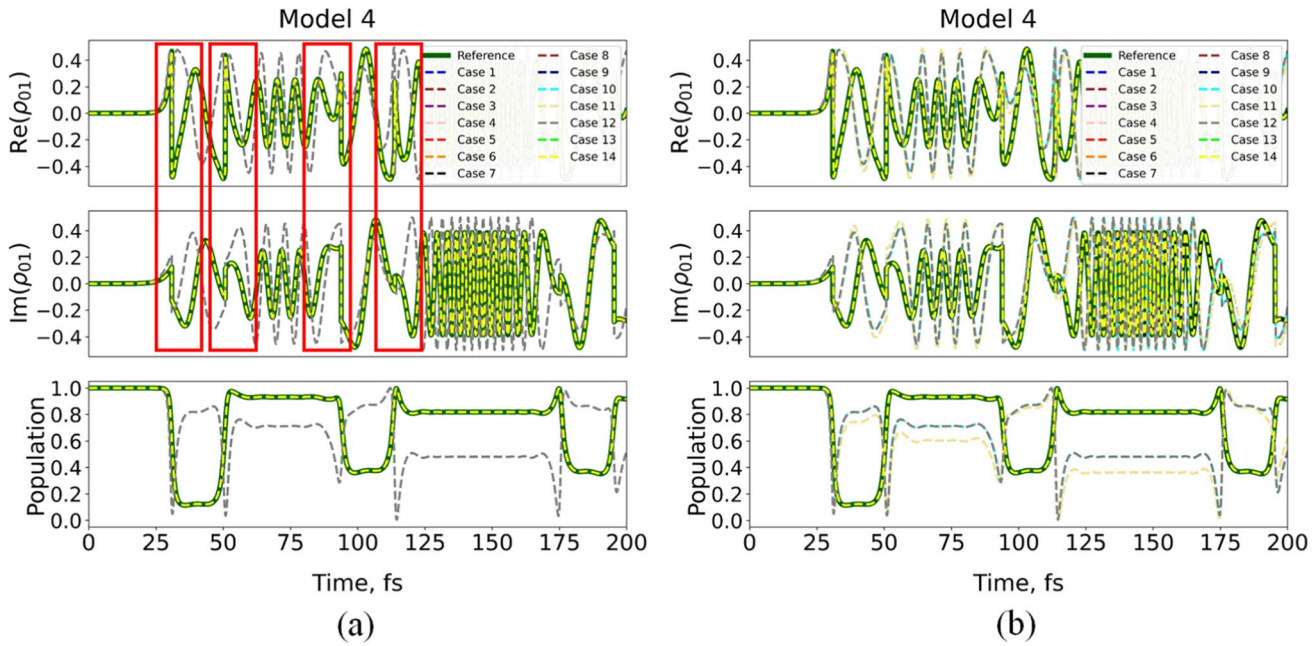

Fig. 5 Evolution of density matrix elements ρ_{00} (population) and ρ_{01} (coherence, real, and imaginary parts) in model Hamiltonian given by Model 4, as computed by different integration schemes. The comparison is illustrated for two integration time steps of (**a**) $\Delta t = 0.001$; and (**b**) $\Delta t = 10.0$. Many methods yield numerically equivalent results, so only few types of curves are visible, especially in the cases with the smallest Δt

oscillations in the Model 1 would decay to populations on each state being close to 0.5 instead of oscillating between the values of 0 and 1. The key step to avoid such errors was to re-initialize the reprojection matrices to the identity matrices, which is consistent with the key approximation in the local diabatization procedure.

To illustrate the error accumulations and to better understand its origin, we analyze the evolution of the density matrix elements. Namely, we consider $\mathrm{Re}(\rho_{00})$, the population of adiabatic state 0, and the components of coherence, $\mathrm{Re}\left(\rho_{01}\right)$ and $\mathrm{Im}(\rho_{01})$, as computed with different integration schemes and different integration time steps (Fig. 5). Figure 5 highlights these properties computed for Model 4, and section S7 of the Supporting Information presents results for other models (Figs. S1–S3). For the smallest integration time step (Fig. 5a), we observe two sets of curves—one, for the reference method and the LD methods (e.g., green and yellow lines), the other—for the heuristic methods (gray dashed). The two sets of curves deviate for some time-intervals and coincide only infrequently. All such deviations contribute to the error shown in Fig. 4. Note that since both population and coherences are bound, and because the error definition, Eq. (45), included time-averaging, the error is also bound at the levels on the order of several units.

A careful examination of the propagated density matrix elements revealed a surprising feature in evolution of the coherence components. Namely, their discontinuities, both for real and imaginary parts (Fig. 5, red boxes). We argue that such discontinuities are introduced by the reprojection operators T. Indeed, consider a simple situation of state switching (e.g., as could occur in Model 1), that is $c_0(t) \to c_1(t+\Delta t)$ and $c_1(t) \to c_0(t+\Delta t)$. If we consider the coherence matrix elements, ρ_{01}, we observe that:

$$\begin{aligned}\rho_{01}(t+\Delta t) &= c_0(t+\Delta t)c_1^*(t+\Delta t)\\ &= c_1(t)c_0^*(t) = \left(c_0(t)c_1(t)\right)^* = \rho_{01}^*(t).\end{aligned} \tag{46}$$

In other words, the imaginary component of the coherence exhibits a discontinuity, a sign flip. In general, the amplitudes change may involve mixing, so the discontinuity would be more general than a sign flip and could involve the real component of coherences as well, as we observe in Fig. 5. In passing, we should clarify that although we observe the discontinuities of the off-diagonal elements of matrix $C_{\mathrm{adi}}C_{\mathrm{adi}}^{+}$, this effect is compensated by the changes of the adiabatic basis functions, so that the full density matrix operator $\hat{\rho} = |\boldsymbol{\psi}_{\mathrm{adi}}\rangle C_{\mathrm{adi}}C_{\mathrm{adi}}^{+}\langle\boldsymbol{\psi}_{\mathrm{adi}}|$ preserves its continuity. Nevertheless, this observation may be important to keep in mind when implementing various decoherence corrections via the density matrix elements, such as those used in the decay of mixing [47–49] and related coherence matrix elements damping schemes [22].

5 Conclusions

In this account, we present a systematic framework for building new integrators for the TD-SE and the QCLE that extend the idea of the LD scheme pioneered by Granucci, Persico and Toniolo. The framework is based on the basis set reprojection combined with the re-initialization of such matrices. The excellent numerical performance of a family of such LD-based integrators confirms the correctness of the underlying theoretical methodology for deriving them. The original LD scheme of Granucci, Persico and Toniolo can be viewed as one of the members of the family of integrators that can be derived from the basis set reprojection approach. We demonstrate that all the derived LD-based integrators are comparable to each other in accuracy, including the original LD scheme and can be used interchangeably. We find that the approach based on evolving the reprojection matrices is unstable and accumulates errors very rapidly due to the underlying approximations. The reprojection matrix re-initialization at every nuclear time step, initially devised within the LD approach, is a critical component for an accurate and stable integration of TD-SE or QCLE.

We demonstrate that the LD algorithms introduce nominal discontinuities in the coherence components. We show that such discontinuities are introduced by the reprojection matrix. Although this matrix does not introduce any discontinuities in populations, it does affect the coherences. This effect may be important to keep in mind when implementing decoherence corrections schemes based directly on modifying coherence matrix elements [50].

We find that the LD-based schemes notably supersede the analogous traditional schemes that directly use vibronic Hamiltonians, H_{vib}, and nonadiabatic couplings. The use of the reprojection matrices is critical for capturing correct qualitative dynamics when trivial crossings are present. No additional state tracking or wavefunction phase corrections are needed. However, even with the reprojection matrices in use, the traditional integration approaches that rely on H_{vib} (and hence explicitly on NACs) yield significantly larger error measure of dynamics as compared to LD-derived ones. We recommend the LD approaches to be used whenever possible. For the model Hamiltonians with the energetics comparable to that of typical molecular Hamiltonians, the electronic TD-SE/QCLE integration time steps could extend up to 100 a.u. (ca. 2.5 fs).

We have derived a Trotter-splitting rotation-based propagator for the TD-SE and the QCLE that works for effective Hermitian Hamiltonians with nonzero off-diagonal elements. We demonstrate that the proper LD algorithms yield comparable accuracy when used with matrix exponential or rotation-based propagation algorithms.

Finally, this work reports an implementation of a large family of the above integrators (both based on LD or H_{vib}, based on matrix exponentiation or rotations algorithms, for TD-SE and QCLE) in the open-source Libra package version v5.4.0. We anticipate that this contribution would be a useful theoretical account on such implementation.

6 Supplementary Information

Detailed scripts and input files used for all types of calculations are available in digital form online at Zenodo repository [51]. The Libra code version 5.4.0 is available online at another Zenodo repository [45].

Supplementary Information The online version contains supplementary material available at https://doi.org/10.1007/s00214-023-03007-7.

Acknowledgements Support of computations is provided by the Center for Computational Research at the University at Buffalo.

Author contributions MS conducted calculations and data analysis, coded data analysis and visualization scripts, prepared figures, assembled electronic data repository, verified the code implementation; AVA implemented integrators in the Libra code, designed and guided the project, acquired funding. All authors wrote and reviewed the manuscript.

Funding This work was carried out with financial support from the National Science Foundation (Grant OAC-NSF-1931366).

Declarations

Conflict of interest The authors declare that they have no conflict of interest.

References

1. Chu W, Zheng Q, Prezhdo OV et al (2020) Low-frequency lattice phonons in halide perovskites explain high defect tolerance toward electron-hole recombination. Sci Adv 6:eaaw7453
2. Chu W, Saidi WA, Zhao J, Prezhdo OV (2020) Soft lattice and defect covalency rationalize tolerance of β-CsPbI3 perovskite solar cells to native defects. Angew Chem Int Ed 59:6435–6441
3. Guo H, Chu W, Zheng Q, Zhao J (2020) Tuning the carrier lifetime in black phosphorene through family atom doping. J Phys Chem Lett 11:4662–4667
4. Akimov AV (2021) Excited state dynamics in monolayer black phosphorus revisited: accounting for many-body effects. J Chem Phys 155:134106
5. Grimaldi G, Crisp RW, ten Brinck S et al (2018) Hot-electron transfer in quantum-dot heterojunction films. Nat Commun 9:2310
6. Jiang X, Zheng Q, Lan Z et al (2021) Real-time GW-BSE investigations on spin-valley exciton dynamics in monolayer transition metal dichalcogenide. Sci Adv 7:3759

7. Shi Y, Prezhdo OV, Zhao J, Saidi WA (2020) Iodine and sulfur vacancy cooperation promotes ultrafast charge extraction at $MAPbI_3/MoS_2$ interface. ACS Energy Lett 5:1346–1354
8. Akimov AV, Asahi R, Jinnouchi R, Prezhdo OV (2015) What makes the photocatalytic CO_2 reduction on N-doped Ta_2O_5 efficient: insights from nonadiabatic molecular dynamics. J Am Chem Soc 137:11517–11525
9. Cheng C, Fang W-H, Long R, Prezhdo OV (2021) Water splitting with a single-atom Cu/TiO_2 photocatalyst: atomistic origin of high efficiency and proposed enhancement by spin selection. J Am Chem Soc Au 1:550–559
10. Niu X, Bai X, Zhou Z, Wang J (2020) Rational design and characterization of direct Z-scheme photocatalyst for overall water splitting from excited state dynamics simulations. ACS Catal 10:1976–1983
11. Gumber S, Agrawal S, Prezhdo OV (2022) Excited state dynamics in dual-defects modified graphitic carbon nitride. J Phys Chem Lett 13:1033–1041
12. Nelson TR, Ondarse-Alvarez D, Oldani N et al (2018) Coherent exciton-vibrational dynamics and energy transfer in conjugated organics. Nat Commun 9:2316
13. Nelson T, Fernandez-Alberti S, Roitberg AE, Tretiak S (2017) Electronic delocalization, vibrational dynamics, and energy transfer in organic chromophores. J Phys Chem Lett 8:3020–3031
14. Andrea Rozzi C, Maria Falke S, Spallanzani N et al (2013) Quantum coherence controls the charge separation in a prototypical artificial light-harvesting system. Nat Commun 4:1602
15. Feit MD, Fleck JA (1983) Solution of the Schrödinger equation by a spectral method II: vibrational energy levels of triatomic molecules. J Chem Phys 78:301–308
16. Raab A, Worth GA, Meyer H-D, Cederbaum LS (1999) Molecular dynamics of pyrazine after excitation to the S_2 electronic state using a realistic 24-mode model Hamiltonian. J Chem Phys 110:936–946
17. Greene SM, Batista VS (2017) Tensor-train split-operator Fourier transform (TT-SOFT) method: multidimensional nonadiabatic quantum dynamics. J Chem Theory Comput 13:4034–4042
18. Gancewski M, Jóźwiak H, Quintas-Sánchez E et al (2021) Fully quantum calculations of O_2–N_2 scattering using a new potential energy surface: collisional perturbations of the oxygen 118 GHz fine structure line. J Chem Phys 155:124307
19. Smith B, Akimov AV (2020) Modeling nonadiabatic dynamics in condensed matter materials: some recent advances and applications. J Phys: Condens Matter 32:073001
20. Wang L, Akimov A, Prezhdo OV (2016) Recent progress in surface hopping: 2011–2015. J Phys Chem Lett 7:2100–2112
21. Tully JC, Preston RK (1971) Trajectory surface hopping approach to nonadiabatic molecular collisions: the reaction of H^+ with D_2. J Chem Phys 55:562–572
22. Tully JC (1990) Molecular dynamics with electronic transitions. J Chem Phys 93:1061–1071
23. Drukker K (1999) Basics of surface hopping in mixed quantum/classical simulations. J Comput Phys 153:225–272
24. Nelson TR, White AJ, Bjorgaard JA et al (2020) Non-adiabatic excited-state molecular dynamics: theory and applications for modeling photophysics in extended molecular materials. Chem Rev 120:2215–2287
25. Floß G, Saalfrank P (2015) The photoinduced E → Z isomerization of bisazobenzenes: a surface hopping molecular dynamics study. J Phys Chem A 119:5026–5037
26. Akimov AV (2016) Libra: An open-source "methodology discovery" library for quantum and classical dynamics simulations. J Comput Chem 37:1626–1649
27. Shakiba M, Smith B, Li W et al (2022) Libra: A modular software library for quantum nonadiabatic dynamics. Softw Impacts 14:100445
28. Akimov AV, Prezhdo OV (2014) Advanced capabilities of the PYXAID program: integration schemes, decoherence effects, multiexcitonic states, and field-matter interaction. J Chem Theory Comput 10:789–804
29. Fernandez-Alberti S, Roitberg AE, Nelson T, Tretiak S (2012) Identification of unavoided crossings in nonadiabatic photoexcited dynamics involving multiple electronic states in polyatomic conjugated molecules. J Chem Phys 137:014512
30. Ryabinkin IG, Izmaylov AF (2017) Mixed quantum-classical dynamics using collective electronic variables: a better alternative to electronic friction theories. J Phys Chem Lett 8:440–444
31. Wang L, Prezhdo OV (2014) A simple solution to the trivial crossing problem in surface hopping. J Phys Chem Lett 5:713–719
32. Temen S, Akimov AV (2021) A simple solution to trivial crossings: a stochastic state tracking approach. J Phys Chem Lett 12:850–860
33. Granucci G, Persico M, Toniolo A (2001) Direct semiclassical simulation of photochemical processes with semiempirical wave functions. J Chem Phys 114:10608–10615
34. Plasser F, Granucci G, Pittner J et al (2012) Surface hopping dynamics using a locally diabatic formalism: charge transfer in the ethylene dimer cation and excited state dynamics in the 2-pyridone dimer. J Chem Phys 137:22A514
35. Meek GA, Levine BG (2014) Evaluation of the time-derivative coupling for accurate electronic state transition probabilities from numerical simulations. J Phys Chem Lett 5:2351–2356
36. Shenvi N, Subotnik JE, Yang W (2011) Phase-corrected surface hopping: correcting the phase evolution of the electronic wavefunction. J Chem Phys 135:024101
37. Mai S, Marquetand P, González L (2018) Nonadiabatic dynamics: the SHARC approach. Wiley Interdiscip Rev Comput Mol Sci 8:e1370
38. Akimov AV (2018) A simple phase correction makes a big difference in nonadiabatic molecular dynamics. J Phys Chem Lett 9:6096–6102
39. Smith B, Akimov AV (2019) A comparative analysis of surface hopping acceptance and decoherence algorithms within the neglect of back-reaction approximation. J Chem Phys 151:124107
40. Dutra M, Garashchuk S, Akimov AV (2023) The quantum trajectory-guided adaptive Gaussian methodology in the Libra software package. Int J Quantum Chem 123:e27078
41. Mandal A, Yamijala SS, Huo P (2018) Quasi-diabatic representation for nonadiabatic dynamics propagation. J Chem Theory Comput 14:1828–1840
42. Akimov AV, Long R, Prezhdo OV (2014) Coherence penalty functional: A simple method for adding decoherence in ehrenfest dynamics. J Chem Phys 140:194107
43. Akimov AV (2022) Fundamentals of trajectory-based methods for nonadiabatic dynamics. In: Reference module in chemistry, molecular sciences and chemical engineering. Elsevier
44. Mukamel S (1995) Principles of nonlinear optical spectroscopy. Oxford University Press, New York
45. Akimov AV, Shakiba M, Smith B, Dutra M, Sato K, Temen S, Li W, Sun X, Stippell L (2023). Quantum-Dynamics-Hub/libra-code: significant refactoring of the code, Local diabatization and more (v5.4.0). Zenodo. https://doi.org/10.5281/zenodo.7846986
46. Verlet L (1967) Computer "Experiments" on classical fluids. I. Thermodynamical properties of Lennard-Jones molecules. Phys Rev 159:98–103

47. Hack MD, Truhlar DG (2001) A natural decay of mixing algorithm for non-Born–Oppenheimer trajectories. J Chem Phys 114:9305–9314
48. Zhu C, Nangia S, Jasper AW, Truhlar DG (2004) Coherent switching with decay of mixing: an improved treatment of electronic coherence for non-Born–Oppenheimer trajectories. J Chem Phys 121:7658–7670
49. Granucci G, Persico M, Zoccante A (2010) Including quantum decoherence in surface hopping. J Chem Phys 133:134111
50. Plasser F, Mai S, Fumanal M et al (2019) Strong influence of decoherence corrections and momentum rescaling in surface hopping dynamics of transition metal complexes. J Chem Theory Comput 15:5031–5045
51. Shakiba M, Akimov AV (2023) AkimovLab/Project_NAMD_Integrators: Project NAMD integrators (v1.0.0). Zenodo. https://doi.org/10.5281/zenodo.7659020

Terms and Conditions

Springer Nature journal content, brought to you courtesy of Springer Nature Customer Service Center GmbH (“Springer Nature”).
Springer Nature supports a reasonable amount of sharing of research papers by authors, subscribers and authorised users (“Users”), for small-scale personal, non-commercial use provided that all copyright, trade and service marks and other proprietary notices are maintained. By accessing, sharing, receiving or otherwise using the Springer Nature journal content you agree to these terms of use (“Terms”). For these purposes, Springer Nature considers academic use (by researchers and students) to be non-commercial.
These Terms are supplementary and will apply in addition to any applicable website terms and conditions, a relevant site licence or a personal subscription. These Terms will prevail over any conflict or ambiguity with regards to the relevant terms, a site licence or a personal subscription (to the extent of the conflict or ambiguity only). For Creative Commons-licensed articles, the terms of the Creative Commons license used will apply.
We collect and use personal data to provide access to the Springer Nature journal content. We may also use these personal data internally within ResearchGate and Springer Nature and as agreed share it, in an anonymised way, for purposes of tracking, analysis and reporting. We will not otherwise disclose your personal data outside the ResearchGate or the Springer Nature group of companies unless we have your permission as detailed in the Privacy Policy.
While Users may use the Springer Nature journal content for small scale, personal non-commercial use, it is important to note that Users may not:

1. use such content for the purpose of providing other users with access on a regular or large scale basis or as a means to circumvent access control;
2. use such content where to do so would be considered a criminal or statutory offence in any jurisdiction, or gives rise to civil liability, or is otherwise unlawful;
3. falsely or misleadingly imply or suggest endorsement, approval , sponsorship, or association unless explicitly agreed to by Springer Nature in writing;
4. use bots or other automated methods to access the content or redirect messages
5. override any security feature or exclusionary protocol; or
6. share the content in order to create substitute for Springer Nature products or services or a systematic database of Springer Nature journal content.

In line with the restriction against commercial use, Springer Nature does not permit the creation of a product or service that creates revenue, royalties, rent or income from our content or its inclusion as part of a paid for service or for other commercial gain. Springer Nature journal content cannot be used for inter-library loans and librarians may not upload Springer Nature journal content on a large scale into their, or any other, institutional repository.
These terms of use are reviewed regularly and may be amended at any time. Springer Nature is not obligated to publish any information or content on this website and may remove it or features or functionality at our sole discretion, at any time with or without notice. Springer Nature may revoke this licence to you at any time and remove access to any copies of the Springer Nature journal content which have been saved.
To the fullest extent permitted by law, Springer Nature makes no warranties, representations or guarantees to Users, either express or implied with respect to the Springer nature journal content and all parties disclaim and waive any implied warranties or warranties imposed by law, including merchantability or fitness for any particular purpose.
Please note that these rights do not automatically extend to content, data or other material published by Springer Nature that may be licensed from third parties.
If you would like to use or distribute our Springer Nature journal content to a wider audience or on a regular basis or in any other manner not expressly permitted by these Terms, please contact Springer Nature at

onlineservice@springernature.com